Theor Chem Account (2008) 120:45–58
DOI 10.1007/s00214-007-0305-7

REGULAR ARTICLE

Structure, vibrational frequencies, ionization energies, and photoelectron spectrum of the para-benzyne radical anion

Vitalii Vanovschi · Anna I. Krylov · Paul G. Wenthold

Received: 17 November 2006 / Accepted: 12 February 2007 / Published online: 9 May 2007
© Springer-Verlag 2007

Abstract Equilibrium structure, vibrational frequencies, and ionization energies of the para-benzyne radical anion are characterized by coupled-cluster and equation-of-motion methods. Vibronic interactions with the low-lying excited state result in a flat potential energy surface along the coupling mode and even in a lower-symmetry C_{2v} structures. Additional complications arise due to Hartree–Fock instabilities and near-instabilities. The magnitude of vibronic interactions was characterized by geometrical parameters, charge localization patterns and energy differences between the D_{2h} and C_{2v} structures. The observed trends suggest that the C_{2v} minimum predicted by several theoretical methods is an artifact of incomplete correlation treatment. The comparison between the calculated and experimental spectrum confirmed D_{2h} structure of the anion, as well as accuracy of the coupled-cluster and spin-flip structures, frequencies and normal modes of the anion and the diradical. Density functional calculations (B3LYP) yielded only a D_{2h} minimum, however, the quality of the structure and vibrational frequencies is poor, as follows from the comparison to high-level wave function calculations and the calculated spectrum. The analysis of charge localization patterns and the performance of different functionals revealed that B3LYP underestimates the magnitude of vibronic interactions due to self-interaction error.

Contribution to the Mark S. Gordon 65th Birthday Festschrift Issue.

V. Vanovschi · A. I. Krylov (✉)
University of Southern California,
Los Angeles, CA 90089-0482, USA
e-mail: krylov@usc.edu

P. G. Wenthold
Department of Chemistry, Purdue University,
West Lafayette, IN 47907-2084, USA

Keywords Para-benzyne radical anion · Photoelectron spectroscopy · Coupled-cluster methods · Density functional theory · Symmetry breaking

1 Introduction

Para-benzyne [1], an intermediate in Bergman cyclization [2], is believed to be a warhead in antitumor enediyne antibiotics [3–5] due to its ability to cause double-strand DNA cleavage and self-programmed cell death or apoptosis [6,7], and extensive studies have been carried out in the past 20 years to understand the factors that control the reaction [8–10]. Originally, it was interest in para-benzyne electronic structure that motivated the development of procedures to generate the corresponding anion for use in photoelectron spectroscopy experiments [11,12]. Recent studies suggested that anionic cycloaromatization reactions are also feasible [13,14] including the anionic version of the Bergman cyclization[15]. Larger sensitivity to substituents [15] suggests that the reactions of the anions might be designed to be more selective than the prototypic non-anionic Bergman cyclization, important for their applications in cancer-DNA damaging drugs.

Previous theoretical studies of the para-benzyne anion [16] predicted strong vibronic interactions (often referred to as pseudo or second-order Jahn–Teller effect) that produce a lower symmetry C_{2v} structure in addition to the D_{2h} minimum. The energy difference between the two structures was found to be highly sensitive to the correlation method, with higher-level models favoring D_{2h}. The analysis of the photoelectron spectrum of the anion [12] supported the assignment of the D_{2h} symmetry, and it was concluded that the lower symmetry structures are artifacts of incomplete correlation

treatment, a well known phenomenon in electronic structure [17]. Interestingly, density functional calculations produced only D_{2h} structures, which was regarded as success of DFT methodology and the authors concluded that "this level of theory is particularly well-suited for computational studies of distonic radical anions derived from diradicals" [16]. The robust behavior of DFT in cases of symmetry breaking has been noted by other researchers as well [18].

The goal of this work is to investigate the performance of coupled-cluster (CC) and equation-of-motion (EOM) methods in this challenging case of strong vibronic interactions and to assess the quality of the ab initio and DFT results by comparing the calculated photoelectron spectrum with the experimental one. We quantify the symmetry lowering by the selected geometrical parameters, charge distributions, and relative energies. In addition, the shape of the potential energy surface along the symmetry breaking coordinate is analyzed. We also present an efficient scheme for calculating ionization energies (IEs) of the anion in the spirit of isodesmic reactions.

Several recent studies [19–21] discussed different aspects of symmetry breaking in electronic structure calculations distinguishing between: (i) purely artefactual spatial and spin symmetry breaking of approximate wave functions, i.e., Löwdin dilemma [22]; (ii) real interactions between closely-lying electronic states that result in lower-symmetry structures, significant changes in vibrational frequencies (see Fig. 1 from Ref. [21]), and even singularities (first order poles) in force constants (e.g., Fig. 3 from Ref. [20]). While the latter is a real physical phenomenon, it may or may not be accurately described by an approximate method. If vibronic interactions are overestimated, calculations may yield incorrect lower-symmetry structure, and vice versa.

Formally, the effect of the interactions between electronic states on the shape of potential energy surface can be described [20] by the Herzberg–Teller expansion of the potential energy of electronic state i:

$$V_i = V_0 + \sum_\alpha < \Psi_i | \frac{\partial H}{\partial Q_\alpha} | \Psi_i > Q_\alpha + \frac{1}{2} \sum_\alpha < \Psi_i | \frac{\partial^2 H}{\partial^2 Q_\alpha} | \Psi_i > Q_\alpha^2 - \sum_\alpha \sum_{j \neq i} \frac{\left(< \Psi_i | \frac{\partial H}{\partial Q_\alpha} | \Psi_j > \right)^2}{E_j - E_i} Q_\alpha^2 \quad (1)$$

where Q_α denotes normal vibrational modes, wave functions Ψ_k and energies E_k are adiabatic wave functions and electronic energies at $Q_\alpha = 0$. The last term, which is quadratic in nuclear displacement — hence *second*-order Jahn–Teller, describes vibronic effects. For the ground state, i.e., when $E_j > E_i$, it causes softening of the force constant along Q_α, which may ultimately result in a lower symmetry structure, e.g., see Fig. 1 from Ref. [21]. The above mentioned poles in force constants originate in the energy denominator.

The formal analysis of the CC and EOM-CC second derivatives by Stanton [20] demonstrated that the quadratic force constant of standard coupled-cluster methods, e.g., coupled-cluster with singles and doubles (CCSD), necessarily contains unphysical terms, which may become significant and spoil the CC force constant in the cases of strongly interacting states. Nevertheless, the standard CC methods are quite reliable for systems exhibiting pseudo Jahn–Teller interactions, as follows from Refs. [20,21], as well as a host of numerical evidence. EOM-CC methods, on the other hand, provide most satisfactory description of the interacting states [20], not at all surprising in view of a multistate nature of EOM. It should be noted that both CC and EOM-CC may exhibit spurious frequencies if the orbital response poles, i.e., coupled-perturbed Hartree–Fock (CPHF) poles, are present due to near-instabilities in the reference, a condition closely related to (i). Perturbative corrections, e.g., as in CCSD(T), do not provide systematic improvement, and often result in wider instability volcanoes [19].

By analyzing the properties of linear response of multi-configurational SCF (MCSCF) and the relationship between response equations and poles' structure, Stanton dispelled a common misconception of relying on multi-reference treatment of systems with strong vibronic interactions [20]. Using the same arguments, he also concluded that DFT describes pseudo Jahn-Teller effects reasonably well. While some numerical evidence [18] seems to support this conclusion, other examples [21] indicated that DFT (B3LYP) tends to *underestimate* the magnitude of vibronic interactions. Our results are in favor of the latter, and we attribute this behavior to self-interaction error.

The structure of the paper is as follows. The next section describes molecular orbitals (MOs) and relevant electronic states of the para-benzyne anion, as well as the nature of vibronic interactions in this system. Section 3 outlines computational details. Section 4 discusses the competition between lower and higher symmetry structures at different levels of theory. Photodetachment spectra are presented in Sect. 5. Different computational strategies for calculating IEs are discussed in Sect. 7. Our final remarks are given in the last section.

2 Molecular orbital picture and the origin of vibronic interactions in the para-benzyne anion

The frontier MOs of the para-benzyne anion and the diradical are shown in Fig. 1. At D_{2h}, the two orbitals belong to different irreps, b_{1u} and a_g, and their density is equally distributed between the two radical centers (C_1 and C_4). At

C_{2v}, both orbitals become a_1, and their densities are localized at different carbons. As in the benzyne diradical, the lowest MO, which hosts two electrons in the anion, is of anti-bonding character with respect to C_1–C_4, whereas the singly occupied MO is bonding. In the case of the diradical, three singlet states and one triplet state are derived from different distributions of two electrons on these two orbitals: X^1A_g, 2^1A_g, 1^1B_{1u}, 2^3B_{1u}. The ground singlet state belongs to the same irrep as the doubly excited singlet, and both have significant multi-configurational character. Likewise, distributing three electrons on these two orbitals in the anion gives rise to two electronic configurations shown in the lower panel of Fig. 1. At D_{2h}, these two determinants are of different symmetry and correspond to two distinct electronic states, X^2A_g and $^2B_{1u}$, separated by the energy gap of about 0.95 eV, as calculated by EOM-CC for electron-attached states (see below). At C_{2v}, both determinants are of A_1 symmetry and, therefore, can interact. This interaction increases the energy separation between the two electronic states that acquire multi-configurational character and, therefore, "softens" the corresponding normal mode in the lower state. If the interaction is sufficiently strong, that is, if the coupling matrix element is large relative to the energy gap between the interacting states, the lower potential energy surface (PES) may develop a lower symmetry minimum. In other words, lowering symmetry stabilizes the lowest electronic state through configurational interaction, and this is the driving force for symmetry breaking.

This analysis of the wave functions of interacting states complements the lessons learned from Eq. (1) and poles' structure of quartic force constants [20,21]. For example, it shows that two factors are important for accurate description of systems with considerable vibronic interactions: (i) balanced description of several possibly multi-configurational wave function (non-dynamical correlation); and (ii) quantitative accuracy in describing excited state ordering (dynamical correlation). Unbalanced treatment may overemphasize the magnitude of vibronic interaction and, therefore, may lead to so-called artefactual symmetry breaking [17]. While (i) can be achieved by multi-configurational self-consistent field (MCSCF), (ii) is much more difficult to satisfy. For example, MCSCF exhibits artificial symmetry breaking in NO_3, which is removed when dynamical correlation is included [23]. Ground-state coupled-cluster methods, e.g., CCSD or CCSD(T), may fail due to the insufficient description of non-dynamical correlation, as it happens in NO_3 [24,25], although they often tackle such challenging systems successfully [26].

The analysis of the MOs and the electronic states of the para-benzyne anion (Fig. 1) suggests a moderate multi-configurational character of the ground state wave function, and this is confirmed by EOM-EA amplitudes (as calculated at EOM-EA-CCSD/6-311+G**) For the D_{2h} structure, the

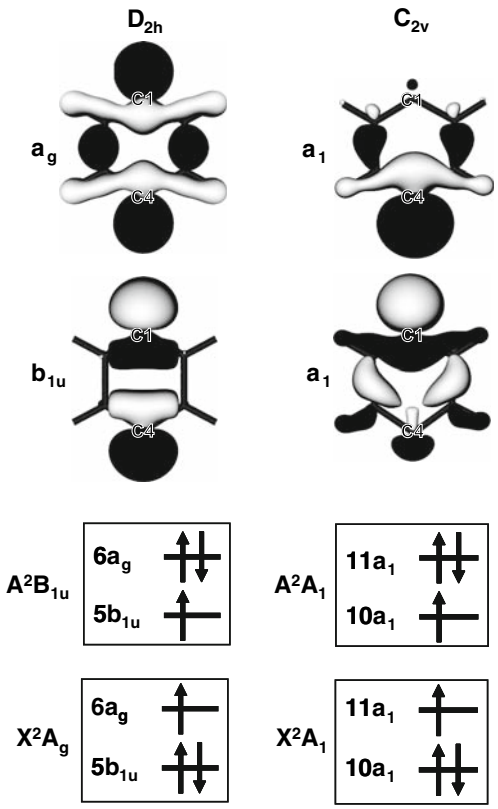

Fig. 1 Frontier MOs and leading electronic configurations of the two lowest electronic states at D_{2h} and C_{2v} structures

EOM coefficient of the leading configuration (the A_g deteminant from Fig. 1 and 2) is 0.86. The three next important configurations have weights of 0.28, 0.26 and 0.07. Likewise, for the C_{2v} structure the weights of the four leading configurations are 0.87, 0.27, 0.16 and 0.15. The EOM-SF-CCSD/6-311+G** amplitudes are similar: the weights of the leading configurations are 0.81 and 0.80 for the D_{2h} and C_{2v} structures, respectively. This confirms minor multi-configurational character of the para-benzyne anion. For comparison, the weights of the four leading configurations of the singlet para-benzyne diradical, which is a truly multiconfigurational system, are 0.57, 0.38, 0.32 and 0.31 and the two leading configurations are double excitations with respect to each other. Thus, we expect ground-state CC methods to be capable of treating $C_6H_4^-$ reasonably well, unlike heavily multiconfigurational wavefunctions, as those of the singlet diradicals [24].

The EOM methods that simultaneously include both dynamical and non-dynamical correlation are particularly attractive for the systems with vibronic interactions. Moreover, as formal analysis of Stanton shows, the pole structure of the exact force constant of Eq. (1) is correctly reproduced within EOM-CC formalism. From the configuration interaction point of view, the balanced description of two important determinants from Fig. 1 is easily provided by several

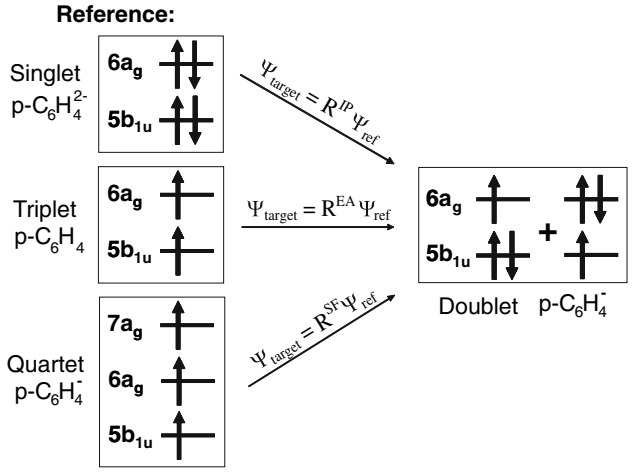

Fig. 2 The two lowest electronic states of $C_6H_4^-$ can be described by: (i) EOM-IP with the dianion reference; (ii) EOM-EA with the triplet neutral p-benzyne reference; (iii) EOM-SF with the quartet p-benzyne anion reference

EOM-CC methods, i.e., ionization potential, electron-attachment, and spin-flip EOM-CC (EOM-EA, EOM-IP, and EOM-SF, respectively), as explained in Fig. 2. All three EOM models include dynamical correlation as well. Their reliability depends on how well the corresponding reference state is described by the single-reference CCSD method and possible (near)-instabilities of the Hartree–Fock references.

3 Computational details

Two basis sets were employed in this work. All the geometry optimizations, frequency calculations and most single point calculations were performed with the 6-311+G** [27,28] basis. Additional single point calculations of IEs used the aug-cc-pVTZ [29] basis.

The choice of reference in our calculations requires additional comments. The ground-state methods [i.e., MP2, CCSD, CCSD(T)], which employ ^2A_g reference, were conducted using pure-symmetry ROHF and UHF references. The $< S^2 >$ values for UHF were 0.869 and 1.226 at D_{2h} and C_{2v}, respectively. The stability analysis revealed several symmetry-breaking triplet instabilities at D_{2h}. The lowest-energy UHF solution is heavily spin-contaminated, $< S^2 >=$ 1.248, and is also of broken symmetry. When employed in the CCSD calculations, the lower-energy broken-symmetry UHF reference yielded *higher* correlated energies, in agreement with our experience (see also footnote 17 in Ref. [20]). Thus, we consider symmetry-pure UHF references to be more appropriate in CC calculations, even though this results in cusps in the PES scans along the $D_{2h} \rightarrow C_{2v}$ distortion. Using symmetry-broken reference at D_{2h} yields continuous curves. In the cases of moderate spin-contamination (as for pure-symmetry UHF references), CCSD is orbital insensitive, however, the (T) correction is often more reliable for ROHF (see, for example, results from Ref. [30]). The optimized-orbital CC models avoid ambiguity of the reference choice for non-variational CCSD, and, in view of UHF instabilities, we consider optimized orbitals coupled-cluster with doubles (OO-CCD) reference to be most appropriate (among the ground-state CC methods) for this system.

References for the EOM calculations (see Fig. 2) were not well behaved either. The closed-shell $^1A_1$ reference for EOM-IP corresponds to the $C_6H_4^{2-}$ dianion, which is unstable. This caused severe convergence problems and we abandoned EOM-IP treatment. The EOM-EA calculations employed the $^3B_{1u}$ state ($^3A_1$ at C_{2v}) of the diradical. Unexpectedly, the corresponding UHF reference develops strong spin contamination at relatively small displacements from D_{2h}: for example, $< S^2 >$=2.026 and 2.468 and D_{2h} and C_{2v}, respectively. This compromises the reliability of EOM-EA-CCSD at C_{2v}. The problem can be resolved by performing the EOM-EA calculations using the OO-CCD triplet reference (EOM-EA-OD). The EOM-SF calculations employ the $^4B_{1u}$ reference ($^4A_1$ at C_{2v}), which can be derived from the $^3B_{1u}$ configuration by placing an additional electron on a σ-like a_g orbital. Despite the similarity to the parent triplet, the quartet reference has been found to be well behaved throughout the whole range of the $D_{2h} \rightarrow C_{2v}$ distortions, e.g., $< S^2 >$=3.776 and 3.779 and D_{2h} and C_{2v}, respectively.

Optimized geometries were obtained at the UHF, ROHF, UHF-CCSD [31], UHF-CCSD(T) [32], OO-CCD [31,33], EOM-EA-CCSD [34], EOM-SF-CCSD [35,36], and B3LYP [37] levels of theory. The latter two methods have produced only D_{2h} structures. For all other methods, two minima were found, and the C_{2v}-D_{2h} energy differences ΔE's were calculated from the corresponding total energies. In addition, ΔE's were calculated by a variety of methods at the UHF-CCSD optimized geometries. The lowest electronically excited states for C_{2v} and D_{2h} structures where computed by EOM-EA-CCSD at the ground state geometries optimized at the same method. We also performed the UHF-CCSD, UHF-CCSD(T), OO-CCD, OO-CCD(T), EOM-EA-CCSD, EOM-SF-CCSD and EOM-EA-OD PES scans along the D_{2h}-C_{2v} displacement coordinate $\mathbf{R}(x)$ defined as:

$$\mathbf{R}(x) = (1 - x) \times \mathbf{r}(D_{2h}) + x \times \mathbf{r}(C_{2v}) \quad (2)$$

where x is a fraction of C_{2v} structure and vector $\mathbf{r}$ denotes Cartesian coordinates of the D_{2h} and C_{2v} structures.

The photodetachment spectra were calculated within double harmonic and parallel normal modes approximations (using normal modes of the anion) by program *PES* [38]. In all spectra calculations, we employed the SF-DFT geometry and frequencies of the singlet state of the diradical [39], while the triplet state was described by CCSD. For the anion, we

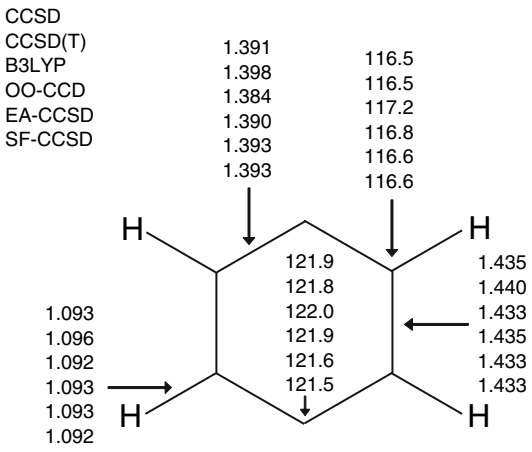

Fig. 3 D_{2h} structures optimized at different levels of theory

used UHF-CCSD and B3LYP geometries and harmonic vibrational frequencies.

Charge distributions were obtained from the natural bond orbital (NBO) analysis [40]. Dipole moments were computed relative to the molecular center of mass. The Mulliken conventions [41] for symmetry labels were used: for both C_{2v} and D_{2h}, the plane of the molecule is *YZ* and the *Z*-axis passes through the two carbons that host the unpaired electrons. Electronic structure calculations were performed using *Q-Chem* [42] and *ACES II* [43].

4 Equilibrium structures, charge distributions, and the $D_{2h} \rightarrow C_{2v}$ potential energy profiles at different levels of theory

This section discusses the D_{2h} and C_{2v} optimized structures, respective energy differences, PES scans, as well as changes in charge distributions upon symmetry lowering. As pointed out by Nash and Squires [16], most theoretical methods predict two minima on the PES, with D_{2h} and C_{2v} symmetries. As follows from the MOs (see Fig. 1), the latter structures are characterized by a localized charge, i.e., are of a distonic type.

The optimized D_{2h} structures are presented in Fig. 3. Figure 4 summarizes differences between the D_{2h} and C_{2v} structures calculated at different levels of theory. For coupled-cluster methods, the changes in geometries between different levels of theory (Fig. 4) are not significant and are smaller for the D_{2h} structure than for C_{2v}. For example, the variation in bond lengths and angles for D_{2h} structures are below 0.02 Å and 2°, respectively. The differences are larger for the C_{2v} structures, possibly because of larger spin-contamination of the doublet and triplet UHF references. The D_{2h} structures calculated by the CC methods with double substitutions, i.e., CCSD, OO-CCD, EOM-EA-CCSD, and

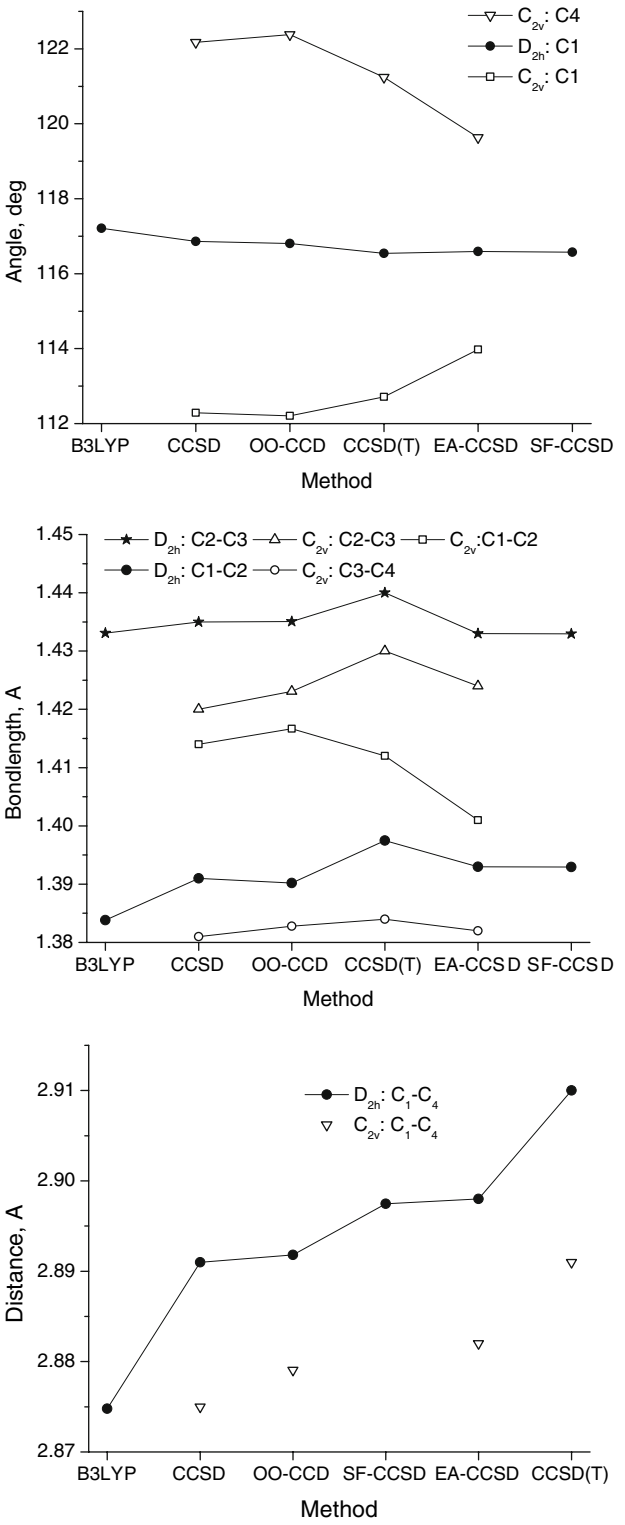

Fig. 4 CCC angles, bonds lengths and the distances between the radical-anion centers calculated by different coupled-cluster methods and B3LYP

EOM-SF-CCSD, are very close to each other, which is reassuring in view of the instability of the doublet UHF reference. The changes in the bond lengths and angles between

CCSD(T) and CCSD are within 0.01 Å and 1°, which is consistent with typical differences for well behaved molecules (Ref. [44]). The largest change due to (T) is observed for the distance between the radical centers. The B3LYP structure is considerably different, e.g., the corresponding C_1–C_4 distance is 0.035 Å shorter than the CCSD(T) value. The above trends suggest that the accuracy of the CC structures is not affected by the HF instabilities and vibronic interactions, and question the reliability of B3LYP results.

The comparison between the D_{2h} and C_{2v} structures allows one to quantify the degree of symmetry lowering at each level of theory. For example, the magnitude of C_{2v} distortions can be characterized by the difference between C_1–C_2 and C_3–C_4, which are identical in D_{2h}. As shown in Fig. 4, the difference in C_1–C_2 between the D_{2h} and C_{2v} structures is largest for CCSD and OO-CCSD and is reduced by the inclusion of triples. At the EOM-EA-CCSD level, it shrinks even further. The C_1–C_2 − C_2–C_3 difference, as well as difference in the C_1 and C_4 angles, follows the same trend. Thus, the magnitude of symmetry breaking is smaller for higher-level methods, or methods that use better references. This, along with the absence of a C_{2v} minimum at the EOM-SF-CCSD level, suggests that its occurrence is artefactual.

The degree of symmetry breaking can also be quantified by the charge localization, which gives rise to a non-zero dipole moment shown in Fig. 5. The corresponding atomic charges calculated using the NBO procedure are consistent with the dipole moment changes, except for ROHF, which may be an artifact of the NBO analysis. In agreement with the trends in structural changes, the charge localization is smaller for more correlated wave functions. Interestingly, the overall dipole moment decreases in spite of increased C_1–C_4 distance. Thus, the charge localization patterns also suggest that the symmetry lowering is an artifact of an incomplete treatment of electron correlation.

Finally, symmetry lowering can be characterized by energy differences (ΔE's) between the D_{2h} and C_{2v} structures summarized in Table 1 and Fig. 6. In addition, several PES scans are shown in Fig. 7. The first part of the table and the upper panel of Fig. 6 summarize single point calculations at the CCSD optimized structures, while the second part and the lower panel of Fig. 6 present energy differences calculated using the respective optimized structures. All ΔE's from Table 1 and Fig. 6 are calculated using symmetry-pure UHF references at D_{2h} (see Sect. 3). Figure 7 shows both the symmetry-pure and symmetry-broken CCSD/CCSD(T) values at D_{2h}. For these methods, the correct-symmetry reference yields lower correlated energies, which results in cusps on the PESs (see Sect. 3). OO-CCD has only one solution at D_{2h} minimum, and the respective curves are smooth.

Similarly to the trends in structures and charge localization, the energy difference between the D_{2h} and C_{2v} structures is also very sensitive to correlation treatment, in agreement with earlier studies [16]. UHF and ROHF place the C_{2v} structure significantly lower (by about 1 eV), than the D_{2h} one, while MP2 gives the almost exactly opposite result. At higher level methods, the energy difference becomes much smaller. At the CCSD and OO-CCD levels, the C_{2v} structure is just a little (<0.1 eV) more stable than the D_{2h} one. Finally, (T) correlation at the CCSD or OO-CCD levels changes the balance and the D_{2h} structure becomes the global minimum. Similarly, at the EOM-EA-CCSD level, D_{2h} is also the lowest minimum. The B3LYP and EOM-SF PES do not have a C_{2v} minimum. Overall, the PES along this distortion is rather flat (due to vibronic interactions): the most reliable estimates of ΔEs between the two CCSD optimized minima range between 0.05 eV (EOM-SF-CCSD) and 0.08 eV [CCSD(T) and OO-CCD(T)]. Optimized-orbital and regular CC methods give similar energy orderings, although OO-CCD and OO-CCD(T) place the D_{2h} structure a little

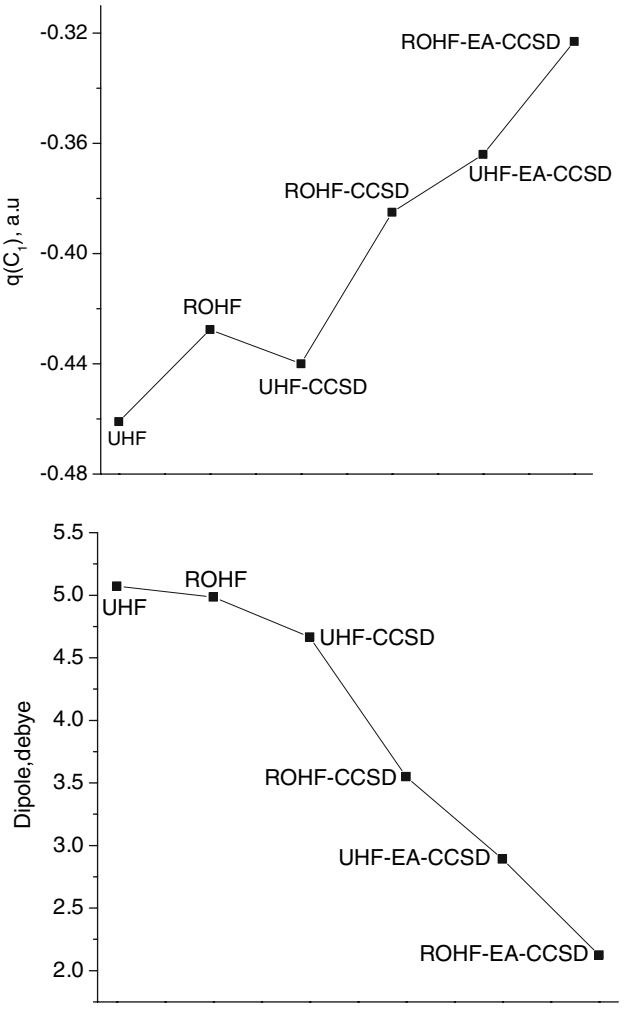

Fig. 5 The NBO charge at C_1 (*top panel*) and dipole moments (*bottom panel*) at the optimized C_{2v} geometries. The ROHF-CCSD and ROHF-EA-CCSD values are calculated at the geometries optimized by the corresponding UHF-based methods

Table 1 Energy differences between the C_{2v} and D_{2h} minima (eV) in the 6-311+G** basis set

Method	UHF	ROHF
At UHF-CCSD optimized geometries		
HF	−0.999	−1.049
MP2	1.191	0.887
CCSD[a]	−0.046(−0.116)	−0.130
CCSD(T)[a]	0.140(−0.052)	0.077
B3LYP	0.070	
5050[b]	−0.149	
OO-CCD	−0.096	
OO-CCD(T)	0.081	
EOM-EA-CCSD	0.086	
EOM-EA-OD	0.050	
EOM-SF-CCSD	0.052	
At the geometries optimized by the corresponding method		
HF	−0.971	−1.039
5050	−0.136	
CCSD	−0.046	
CCSD(T)	0.140	
OO-CCD	−0.097	
EOM-EA-CCSD	0.071	

Negative values correspond to the C_{2v} minimum being lower. ZPEs are not included.

[a] Calculated using symmetry-pure and symmetry-broken (values in parenthesis) doublet UHF references at D_{2h}

[b] DFT functional with 50% of the HF exchange

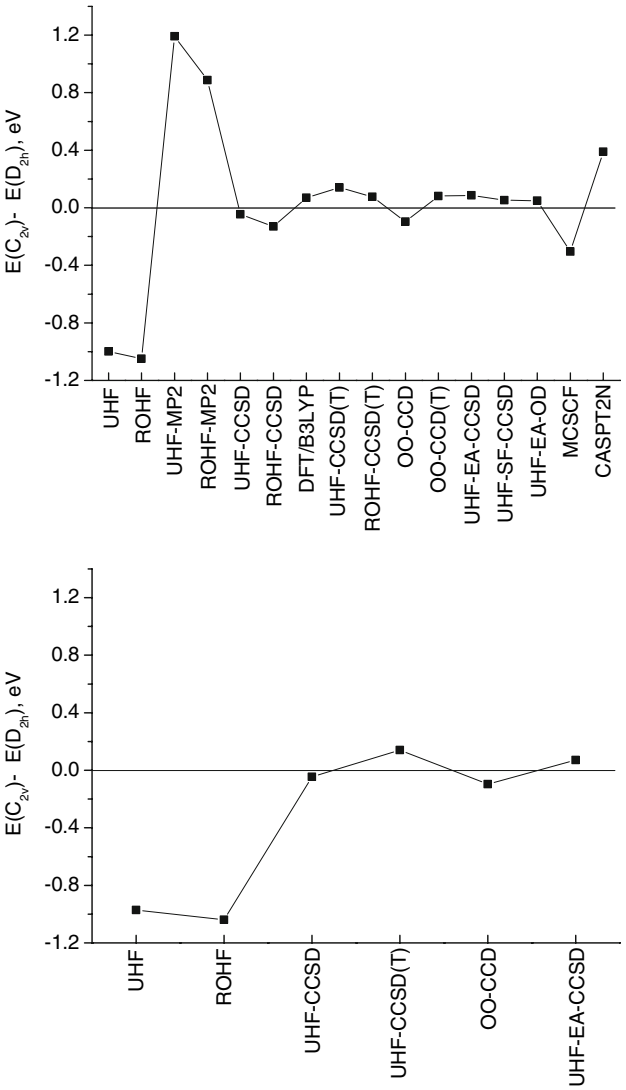

Fig. 6 Energy differences between the C_{2v} and D_{2h} structures ($6-311+G^{**}$ basis). *Upper panel* calculated using the UHF-CCSD optimized geometries. MCSCF and CASPT2N employ the MCSCF geometries and are from Ref. [16]. *Lower panel* calculated at the respective optimized geometries

higher than the corresponding CC methods based on the Hartree–Fock reference. EOM-SF behave similarly to EOM-EA.

Similar trends, although with larger variations, were observed for multi-reference methods, e.g., MCSCF and CASPT2. The previous study [16] reported the energy differences between the C_{2v} and D_{2h} structures calculated by multi-reference methods as −0.286 eV for MCSCF(9,8)/cc-pVDZ and 0.388 for CASPT2N/cc-pVDZ. Thus, only when dynamical correlation is included in a multi-reference method, the D_{2h} structure becomes the lowest in energy.

As follows from Table 1, using different optimized geometries has only a minor effect on ΔE's. For example, the energy differences calculated at the CCSD optimized geometries are within 0.03 eV to those calculated using the structures optimized at the same level of theory, and the observed trends are the same.

Thus, the presented ΔE's exhibit the same trend as the optimized geometries and charge localization patterns — the more correlation we add the more stable the D_{2h} structure becomes.

Energy profiles from Fig. 7 give more detailed information on the shape of the PES. Due to the HF instabilities, the CCSD and CCSD(T) curves are discontinuous, unless the symmetry-broken UHF reference is used at D_{2h}. Apart from the cusp, the shapes of the OO-CCD and CCSD curves are surprisingly similar. The difference becomes more profound when triples are included: the OO-CCD(T) curve smoothly descends towards the D_{2h} minimum, while the CCSD(T) curve is gradually climbing up all the way till the final drop at D_{2h}. Even though the corresponding $D_{2h} \rightarrow C_{2v}$ ΔE's are close, the shape of the EOM-SF-CCSD and OO-CCD(T) curves are quite different: the former is much flatter at D_{2h} than the latter. The EOM-EA-CCSD curve parallels EOM-SF-CCSD around D_{2h}, but soon becomes spoiled by the instability in the triplet reference. Using optimized orbitals triplet reference solves the problem of HF instability and the EOM-EA-OD curve is very similar to the EOM-SF-CCSD

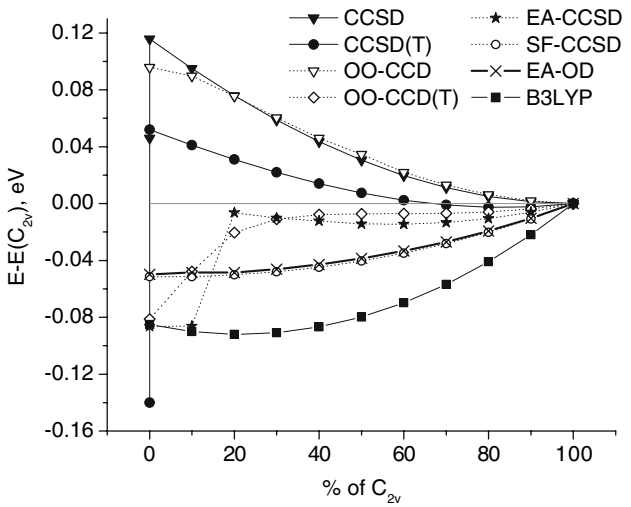

Fig. 7 The potential energy profiles along the D_{2h}-C_{2v} scans. At the D_{2h} structure, CCSD and CCSD(T) energies are calculated using symmetry-broken and pure-symmetry UHF references (see Sect. 3)

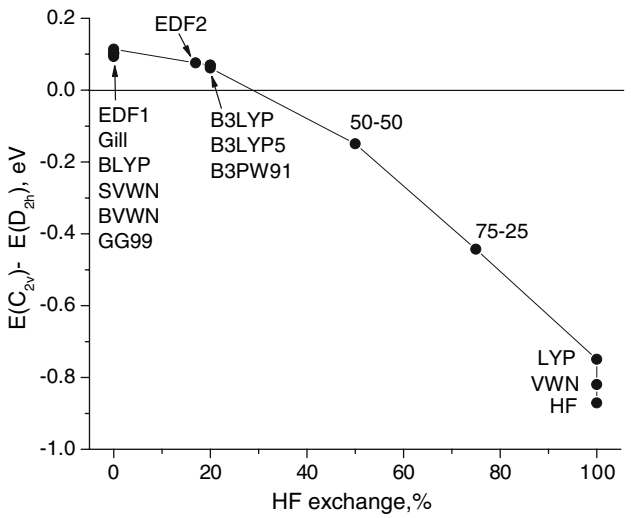

Fig. 8 Energy differences between the D_{2h} and C_{2v} minima (using the CCSD structures) calculated using different density functionals

one. The B3LYP curve is steeper than the EOM-SF one, consistent with large value of the corresponding frequency (see next section). Overall, Fig. 7 demonstrates that describing the shape of PES is more challenging than calculating energy difference between two minima. One should expect considerable differences in the corresponding vibrational frequency. Note that the analytic CCSD or CCSD(T) frequencies would differ dramatically from those calculated by finite differences: the analytic frequencies will characterize the curvature of the PES corresponding to the symmetry-pure reference, whereas finite difference calculations will sample the cusp.

To conclude, the analysis of the equilibrium structures, charge distributions, and energy differences calculated at different levels of theory suggests that the C_{2v} minimum is an artifact of incomplete treatment of electron correlation and HF instabilities in the doublet or triplet references. The strong vibronic interactions result in rather flat PES along the $D_{2h} \rightarrow C_{2v}$ distortion. In the next section, we present our calculations of the photoelectron spectrum, which allows us to assess the quality of calculated geometries and to unambiguously determine the symmetry of the anion (Fig. 8).

5 Vibrational frequencies and the photoelectron spectrum of para-$C_6H_4^-$

Photoelectron spectroscopy is a very sensitive structural tool. The spectra depend on equilibrium geometries, frequencies and normal modes of the initial (radical anion) and target (diradical) states. The equilibrium geometries were discussed in the previous section. The vibrational frequencies of the anion (at D_{2h}) and the diradical are given in Table 2. The CCSD and B3LYP frequencies of the anion appear to be similar, except for the lowest b_{1u} mode that describes $D_{2h} \rightarrow C_{2v}$ displacements and is most affected by vibronic interactions. This mode also exhibits the largest change relative to the neutral, i.e., it is considerably softer in $C_6H_4^-$. The B3LYP frequency is 40% higher than the CCSD value, in favor of our assumption that B3LYP underestimates the magnitude of vibronic interaction. Unfortunately, the only significant vibrational progressions present the Franck–Condon factors (see Sect. 3) are those for fully-symmetric normal modes that exhibit displacements relative to the anion. Modes with significant frequency change, such as the above b_{1u} mode, yield much smaller features that are likely to be buried under major progressions, as it happens for the para-benzyne anion.

The electron photodetachment spectrum of the para-benzyne radical anion reported by Wenthold and coworkers [12] consists of the two overlapping bands corresponding to the singlet (X^1A_g) and triplet ($^3B_{1u}$) states of the diradical with the origins, i.e., electron affinities (EAs), at 1.265 ± 0.008 and 1.430 ± 0.015 eV, respectively. Long vibrational progressions for frequencies at 635 ± 20 and 990 ± 20 cm^{-1} (assigned to the singlet band), at 610 ± 15 and 995 ± 20 cm^{-1} (assigned to the triplet band), as well as a hotband at 615 ± 30 cm^{-1} were reported. For both the singlet and the triplet bands, the lower (about 600 cm^{-1}) and the higher (about 1,000 cm^{-1}) energy progressions were assigned to symmetric ring deformation and ring breathing, respectively. These bands, four lowest a_g vibrations, are also present in all the computed spectra. Including the lowest b_{1u} mode resulted in very small features, completely obscured by the dense lines of major progressions.

In the original paper [12], the normal displacements were derived from the fitting procedure. Table 3 and Fig. 9 compare these values with the shifts computed in this work from the

Table 2 Vibrational frequencies of the para-benzyne radical anion and the diradical

Symmetry	X^2A_1[a]	X^2A_1[b]	a^3B_{1u}[a]	X^1A_1[c]
a_g	3137	3085	3221	3317
a_g	1471	1434	1565	1440
a_g	1189	1175	1166	1202
a_g	992	981	1028	1065
a_g	624	631	615	660
a_u	879	917	920	994
a_u	380	398	368	450
b_{1g}	691	721	810	722
b_{2g}	1120	890	871	961
b_{2g}	647	601	437	616
b_{3g}	3114	3061	3207	3302
b_{3g}	1579	1549	1652	1738
b_{3g}	1297	1284	1300	1327
b_{3g}	608	612	585	597
b_{1u}	3111	3056	3206	3300
b_{1u}	1445	1425	1471	1511
b_{1u}	1071	1060	1046	1101
b_{1u}	452	639	947	973
b_{2u}	3136	3082	3220	3316
b_{2u}	1331	1332	1375	1448
b_{2u}	1189	1203	1267	1254
b_{2u}	1027	1020	1081	1076
b_{3u}	715	718	753	796
b_{3u}	422	447	400	477

[a] Calculated at UHF-CCSD/6-311 + G**
[b] Calculated at B3LYP/6-311 + G**
[c] From Ref. [39], SF-5050/6-31G**

Table 3 Displacements in normal modes upon ionization, $A * \sqrt{amu}$

Method	Singlet		Triplet	
	ν_5^a	ν_4^b	ν_5^a	ν_4^b
Exp. fit[c]]	−0.44	−0.14	0.76	−0.12
CCSD[d]	−0.49	−0.21	−0.69	−0.09
CCSD(T)[d]	−0.50	−0.27	−0.71	−0.14
EOM-EA-CCSD[d]	−0.49	−0.22	−0.70	−0.10
OO-CCD[d]	−0.49	−0.21	−0.69	−0.09
DFT/B3LYP[d]	−0.47	−0.17	−0.67	−0.05
DFT/B3LYP[e]	−0.40	−0.29	−0.60	−0.23

[a] Ring deformation
[b] Ring breathing
[c] Ref. [12]
[d] using the CCSD normal modes
[e] using the DFT/B3LYP normal modes

corresponding D_{2h} optimized geometries and normal modes of the anion. The triplet and the singlet states of the diradical

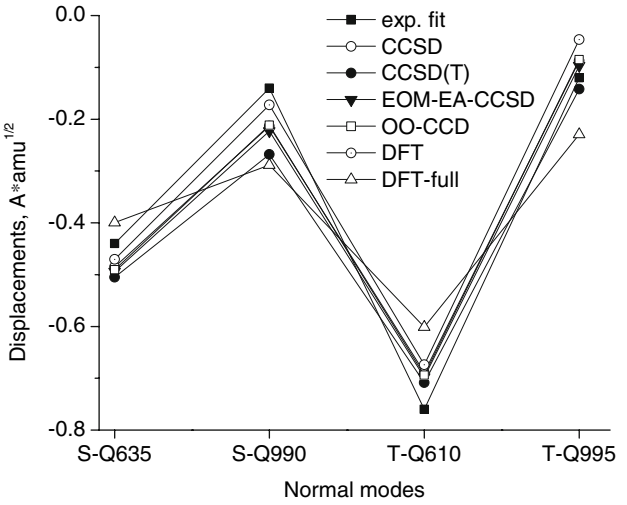

Fig. 9 Displacements along the normal modes upon ionization (D_{2h} structure)

are described by the CCSD and spin-flip DFT methods, respectively (see Sect. 3). The computed CCSD shifts are very close to those derived from the experiment. Values obtained with the CCSD normal modes and different equilibrium structures [e.g., CCSD(T), EOM-EA-CCSD, OO-CCD, and B3LYP] are quite similar to each other. However, the full B3LYP shifts (the last line in Table 3), i.e., those computed using the B3LYP normal modes and B3LYP equilibrium structures, are much larger for the ring breathing mode, which will result in a longer progression.

Finally, Fig. 10 compares the calculated and experimental photodetachment spectra. The upper panel of Fig. 10 shows the singlet and triplet bands of the spectrum for the D_{2h} structures calculated using the CCSD description of the anion. To compare with the experimental spectrum, the scaled intensities of the singlet and triplet bands were added together. Two scaling coefficients were determined from the following conditions: (i) the combined spectrum is normalized to 1; and (ii) the intensity of peak number 3 in the experimental and the calculated spectra coincide. The experimental spectrum was normalized to 1 as well. The bottom part of Fig. 10 compares the computed D_{2h} and the experimental spectra. The agreement between the two spectra is excellent: the computed spectrum has the same features as the experimental one and differs only slightly in the peaks' intensities. Figure 11 shows the spectrum calculated for the C_{2v} CCSD structure, which is markedly different — it features additional progressions that are not present in the experimental spectrum. They correspond to the ring deformation band and the combination bands involving this mode. To conclude, an excellent agreement between the spectrum calculated using the D_{2h} structure and the experimental one, along with significant

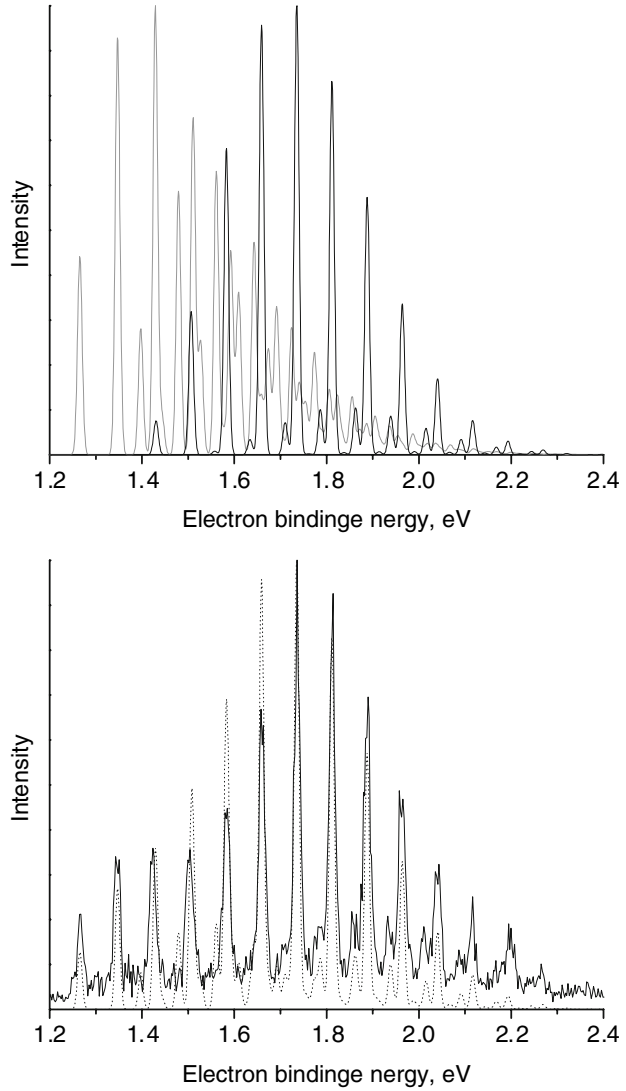

Fig. 10 *Top* Singlet (*solid line*) and triplet (*dotted line*) bands of the electron photodetachment spectrum for D_{2h} using the CCSD equilibrium geometries and frequencies of the anion. *Bottom* the experimental (*solid line*) and the calculated (*dotted line*) spectra for D_{2h} using the CCSD structure and normal modes

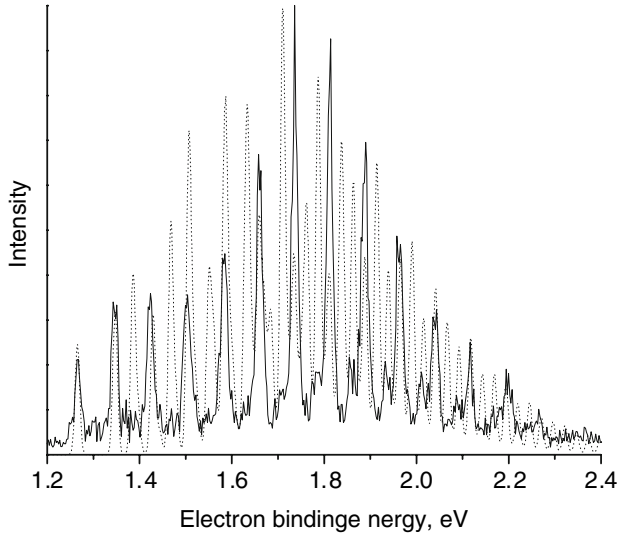

Fig. 11 The experimental (*solid line*) and the calculated (*dotted line*) spectra for C_{2v} using the CCSD structure and normal modes

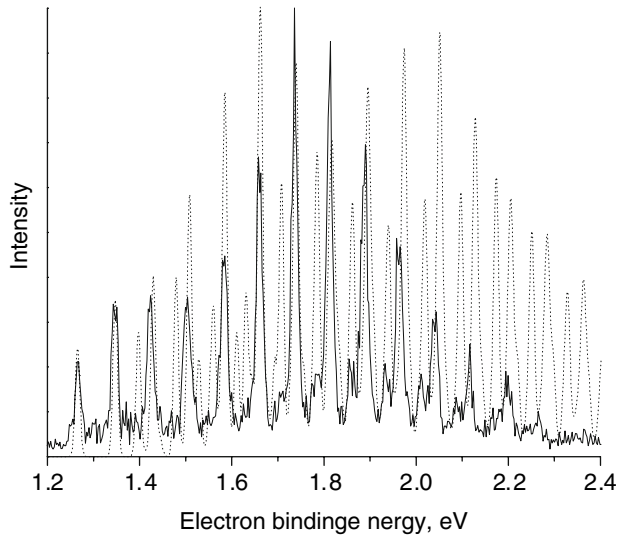

Fig. 12 The experimental (*solid line*) and the calculated (*dotted line*) spectra for D_{2h} using the B3LYP structure and normal modes

differences between D_{2h} and C_{2v}, unambiguously proves the D_{2h} structure of the para-benzyne radical anion. Moreover, it also confirms high quality of the CCSD equilibrium structure and frequencies for the anion, as well as the accuracy of the spin-flip description of the diradical. We also calculated the spectrum using the B3LYP optimized geometries and frequencies for p-$C_6H_4^-$ (and the same structures and frequencies for the diradical, as above). The resulting spectrum (Fig. 12) has significantly different ratio of intensities for the two main bands and much longer progressions. Thus, even though DFT correctly predicts symmetry of the para-benzyne radical anion, the overall structure is of poor quality. The reasons for this are discussed below.

6 DFT self-interaction error and vibronic interactions

The analysis of equilibrium structures, charge localization, and energy differences between D_{2h} and C_{2v} structures presented in Sect. 4 demonstrated that the magnitude of symmetry breaking decreases when higher level methods are employed. Moreover, the PES scans and the analysis of UHF references strongly suggest that the existence of a C_{2v} minimum is an artifact. Indeed, EOM-SF-CCSD, the only CC method that employs a well-behaved UHF reference (that is, symmetry-pure, not strongly spin-contaminated and stable), yields only a D_{2h} minimum and a smooth PES. The EOM-EA-OD potential energy profile parallels the EOM-SF one.

Finally, modeling of the photoelectron spectrum ruled out the C_{2v} structure. Thus, we conclude that symmetry breaking in p-$C_6H_4^-$ is purely artefactual.

DFT/B3LYP appears to be more robust with respect to this artefactual symmetry breaking as it yields only a D_{2h} structure. The important question is *why*, and whether or not one should consider DFT a reliable tool for modeling systems with strong vibronic interactions. Detailed benchmark studies (e.g., Ref. [18]) provide many examples of DFT giving "the right answer" for difficult symmetry breaking systems. Stanton explained these observations by making connections between DFT response theory, TD-DFT excitation energies and their Tamm–Dancoff approximation (footnote 23 in Ref. [20]), and concluded that DFT describes pseudo Jahn–Teller effects reasonably well "for the right reason", that is, because the poles appear in approximately the right places. Other examples, however, suggested that DFT might actually underestimate the magnitude of vibronic interactions [21]. To complicate matters even further, we would like to mention the dehydro-meta-xylylene anion (DMX^-) for which DFT yields low symmetry (C_s or C_2) equilibrium geometries [26], while wave function based methods predict planar C_{2v} structures [45].

To gain insight, we begin by analyzing the character of interacting electronic states in p-$C_6H_4^-$ and DMX^- at symmetric and symmetry-broken geometries. As described in Sects. 2 and 4, the two interacting states of p-$C_6H_4^-$ have the excess charge equally delocalized between two radical centers (C_1 and C_4) at D_{2h}, whereas C_{2v} distortions result in the charge localization at one of the carbons. DMX^- shows exactly the opposite behavior [45,26]: at the planar C_{2v} geometries, most of the excess charge resides on the σ-radical center, whereas C_2 or C_s displacements facilitate the flow of the charge into the π-system. Thus, in both cases B3LYP favors the structures with more delocalized excess charge, which immediately brings about the infamous H_2^+ example [46]. While HF dissociation curve for a one-electron H_2^+ is exact, many DFT methods result in quasi-bound potential energy curves and with errors as large as 50 kcal/mol! This happens because DFT over-stabilizes the solutions with an electron being equally split between the two hydrogens, which is an artifact of self-interaction error (SIE) present in many functionals [47–49]. SIE is considerably larger in systems with odd number of electrons. Self-interaction energy, Coulomb interaction of an electron with itself, is always positive, and electron delocalization lowers its magnitude thus causing artificial stabilization of delocalized configurations. Other well understood examples of artificial stabilization of delocalized states due to SIE include underestimated barriers for radical reactions, dissociation of cationic radicals, and mixed-valence transition metal dimers [49].

As shown in Ref. [48], the magnitude of SIE in H_2^+ strongly depends on the distance between the atoms, varying from a negligibly small value around the equilibrium to 55 kcal/mol (B3LYP) at the dissociation limit. The charge-bearing radical centers in the para-benzyne radical anion are 2.9 Å apart. At this distance, the H_2^+ curve exhibits as much as 60% of its maximum SIE. This suggests substantial SIE in the Para-benzyne radical anion.

To test this assumption, we computed energy differences between the D_{2h} and C_{2v} minima (using the CCSD optimized geometries) employing functionals with a varying fraction of HF exchange. The results are shown in Fig. 8. The trend is clear: the relative stabilization of the D_{2h} structure is inversely proportional to the fraction of the HF exchange in the functional, and, consequently, is proportional to SIE. Combining different correlation functionals with the fixed fraction of the HF exchange has little effect on the ΔE's, for example, all functionals with 0% HF exchange yield approximatly the same D_{2h}-C_{2v} enegry separition. Therefore, we conclude that for DFT, the strengths of vibronic interactions and, consequently, a relative ordering of the D_{2h} and C_{2v} structures, are governed by SIE. Thus, B3LYP yields the right structure for the "wrong reason". Therefore, it is not at all surprising that the quality of the B3LYP structure and the shape of PES is relatively poor, as follows from the comparison of the computed photoelectron spectrum with the experimental one. In DMX^-, B3LYP yields the wrong structure, but for the same "right reason" (SIE). Therefore, B3LYP (or any functional with SIE) is not a reliable method for the systems with strong vibronic interactions that affect charge localization patters, or when the interacting states are characterized by considerably different charge distributions.

7 Calculation of electron affinities of p-benzyne

Different strategies for calculating electron affinities in problematic open-shell systems were discussed in Ref. [26]. The simplest "brute-force" approach, i.e., to take the difference between the total energies of the anion and the neutral calculated at the same level of theory, can give accurate values only if the errors in the corresponding total energies are very small (which can be achieved only at very high levels of theory), or if both species are described on the equal footing by the method and errors in the total energies cancel out. The latter is difficult to achieve in the case when both the neutral and anion wave functions have a complicated open-shell character. For example, the singlet state of the diradical is significantly multi-configurational and it would be described less accurately than the anion by single reference methods. The triplet state of the diradical, however, is single-configurational and can be described by single-reference methods with approximately the same accuracy as the doublet. Thus, triplet EAs calculated by energy differences employing correlated single-reference methods are more reliable than singlet

EAs. The latter can be accurately computed by subtracting the experimental (or a calculated by an appropriate method) singlet—triplet gap from the calculated triplet electron affinity. This approach was used for calculating EAs of triradicals [45,26] and diradicals [50]. Below we demonstrate that this scheme in the spirit of isodesmic reactions indeed yields accurate singlet EAs.

EAs calculated at different levels of theory for the singlet and the triplet states of the diradical are presented in Table 4 and Fig. 13. The first two columns present triplet and singlet EAs computed by energy differences. The last column presents singlet EA calculated from the corresponding triplet EA and the best theoretical estimate of the singlet–triplet gap. For the triplet state, which is predominantly single-configurational, even relatively low level methods using a moderate basis, e.g., B3LYP and MP2 in 6-311+G**, yield reasonable EAs, e.g., within 0.11 and 0.07 eV from the experiment, respectively. For the singlet state, however, EAs calculated by DFT and MP2 are 1.03 and 0.67 eV off, because these methods are not appropriate for the multi-configurational wave function of the singlet. Note that such brute-force approach reverses the states ordering in the diradical even at the CCSD level. For both states coupled-cluster methods, especially with triples' corrections, are in a reasonable agreement with the experimental values. For example, ROHF-CCSD(T) is within 0.16 eV for triplet and within 0.05 eV for singlet.

Table 4 Electron affinities (eV) of the a^3B_{1u} and X^1A_g states of the Para-benzyne diradical

Method	Triplet EA	Singlet EA	Singlet EA[a]
Experiment	1.430	1.265	
Experiment-ZPE	1.375	1.140	
6-311+G** basis			
B3LYP	1.481	2.172	1.310
UHF	−0.994	2.679	−1.165
UHF-MP2	1.547	0.467	1.376
UHF-CCSD	0.893	1.659	0.722
UHF-CCSD(T)	1.207	1.085	1.036
ROHF	−1.148	2.356	−1.319
ROHF-MP2	2.053	0.914	1.882
ROHF-CCSD	0.872	1.629	0.701
ROHF-CCSD(T)	1.216	1.094	1.045
OO-CCD	0.875	1.644	0.704
OO-CCD(T)	1.210	1.080	1.039
aug-cc-pVTZ basis			
ROHF	−1.199	2.297	−1.370
ROHF-MP2	2.266	1.010	2.095
ROHF-CCSD	0.998	1.766	0.827
ROHF-CCSD(T)	1.395	1.258	1.224

[a] Calculated by using triplet EA and the singlet–triplet gap from Ref. [51]

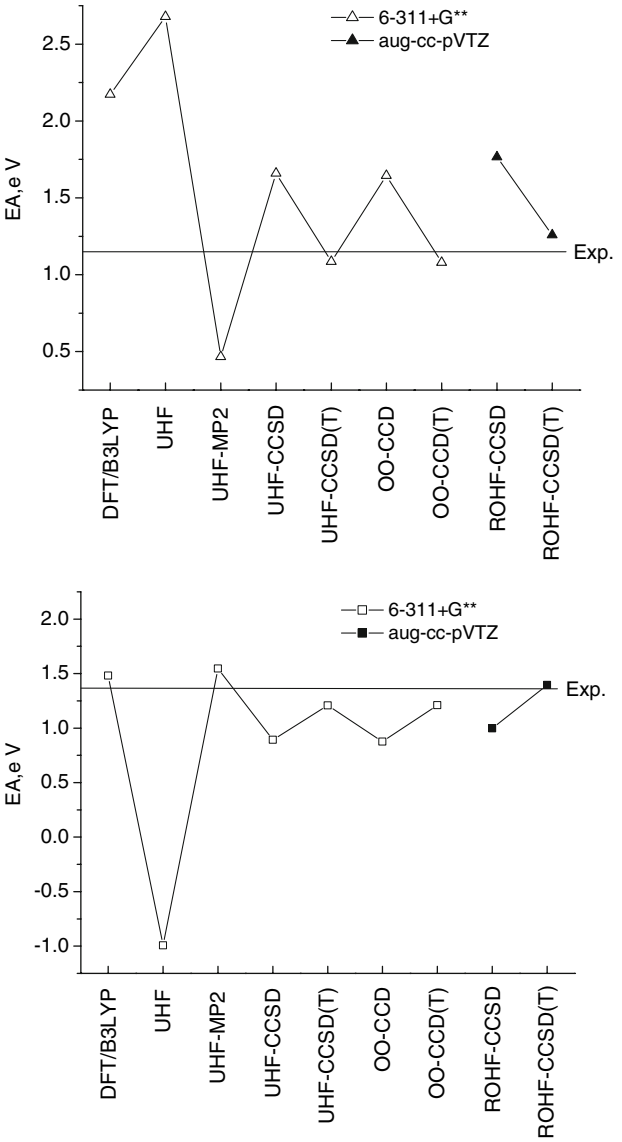

Fig. 13 Adiabatic electron affinities calculated by energy differences for the singlet (*top panel*) and triplet (*bottom panel*) state of the Para-benzyne diradical

For quantitative thermochemical results, larger basis sets are required. We performed additional coupled-cluster calculations with the aug-cc-pVTZ basis (see Table 4). EA for the triplet calculated by CCSD(T) is within 0.02 eV from the experimental one, as expected for this method. However, the singlet CCSD(T) value is 0.12 eV off, because of the poor description of the multi-configurational singlet state by ground-state single-reference methods.

By employing the best theoretical estimate for the singlet-triplet gap in para-benzyne, i.e., 0.171 eV from Ref. [51], singlet EA calculated from the CCSD(T) triplet value is within 0.08 eV from the experiment, as compared to 0.12 eV

for the brute-force approach. As follows from the excellent agreement of triplet EA, the accuracy of singlet EA can be improved by refining the value of the singlet–triplet gap.

8 Conclusions

The shape of ground-state PES of $C_6H_4^-$ is strongly affected by the vibronic interactions with a low-lying excited state. The magnitude of vibronic interactions depends crucially on the the energy gap and couplings between the interacting states. Complicated open-shell character of the wave functions of the interacting states and HF instabilities challenge ab initio methodology: the shape of PES along the vibronic coupling coordinate differs dramatically for different methods. For example, many wave function based methods predict vibronic interactions to be strong enough to result in a lower-symmetry C_{2v} minimum, in addition to the D_{2h} structure. EOM-SF-CCSD and B3LYP predict only a single minimum, however, the curvature of the surface is quite different.

The degree of this symmetry lowering can be quantified by structural parameters (e.g., the magnitude of nuclear displacements), charge localization and the resulting dipole moment, as well as energy difference between the two minima. We found that the magnitude of symmetry breaking (as characterized by the above metrics) decreases when higher-level methods are employed. For example, the dipole moment of the C_{2v} structure decreases in the HF→CCSD→EOM-EA-CCSD series. Likewise, coupled-cluster methods with triples corrections as well as EOM-EA/SF-CCSD predict that D_{2h} is a lower energy structure. Moreover, EOM-SF predicted only D_{2h} minima. Calculation of the potential energy profiles along the $D_{2h}\rightarrow C_{2v}$ distortion and the stability analysis of UHF references allowed us to attribute the lower-symmetry minimum to the incomplete treatment of electron correlation and UHF instabilities.

The quality of D_{2h} structure was assessed by comparing the computed photoelectron spectrum against the experiment. The spectrum calculated using the CCSD description of the anion and the triplet diradical and the SF-DFT results for the singlet diradical is in an excellent agreement with the experimental one, which is particularly encouraging in view of its dense and complicated nature. The spectrum calculated using the C_{2v} geometry and frequencies is markedly different, which allows us to rule out the C_{2v} structure.

As pointed out in earlier studies [16], B3LYP appears to be robust w.r.t. this artefactual symmetry breaking, and yields only D_{2h} structure. The analysis of the structure and the potential energy profile along the $D_{2h}\rightarrow C_{2v}$ distortion reveals that the structure and the curvature are considerably different from those calculated by reliable wave function methods. Moreover, the computed spectrum differs significantly from the experimental one. The shape of the surface, as well as the corresponding harmonic frequency reveals that B3LYP underestimates the magnitude of vibronic interactions, as pointed out earlier by Crawford and coworkers [21]. Further analysis allowed us to attribute the failure of B3LYP to the self-interaction error. A similar behavior (that yielded seemingly different result) was observed in DMX^-, where SIE resulted in B3LYP overestimation of vibronic interactions and, consequently, a lower symmetry structure. In both cases, large SIE originates in significant changes in charge localization patterns along symmetry breaking coordinate. Thus, B3LYP is not a reliable method for systems where vibronic interactions are coupled to different charge localization patterns, as happens in distonic radical and diradical anions.

Acknowledgements This work was conducted in the framework of the Center for Computational Studies of Electronic Structure and Spectroscopy of Open-Shell and Electronically Excited Species supported by the National Science Foundation through the CRIF:CRF CHE-0625419 + 0624602 + 0625237 grant. AIK and PGW also gratefully acknowledge support of the National Science Foundation through the CHE-0616271 and CHE-0454874 grants, respectively.

References

1. Wenk HH, Winkler M, Sander W (2003) Angew Chem Int Ed Engl 42:502
2. Jones RR, Bergman RG (1972) J Am Chem Soc 94:660
3. Lee MD, Dunne TS, Siegel MM, Chang CC, Morton G0, Borders DB (1987) J Am Chem Soc 109:3464
4. Borders DB, Doyle TW (eds) (1995) Enediyne antibiotics as antitumor agents. Marcel Deekker, New York
5. Maeda H, Edo K, Ishida N (eds) (1997) Neocarzinostatin: the past, present, and future of an anticancer drug, Springer, New York
6. Schottelius MJ, Chen P (1996) Angew Chem Int Ed Engl 3:1478
7. Hoffner J, Schottelius MJ, Feichtinger D, Chen P (1998) J Am Chem Soc 120:376
8. Nicolaou KC, Smith AL (1992) Acc Chem Res 25:497
9. Bowles DM, Palmer GJ, Landis CA, Scott JL, Anthony JE (2001) Tetrahedron 57:3753
10. Zeidan T, Manoharan M, Alabugin IV (2006) J Org Chem 71:954
11. Wenthold PG, Hu J, Squires RR (1996) J Am Chem Soc 118:11865
12. Wenthold PG, Squires RR, Lineberger WC (1998) J Am Chem Soc 120:5279
13. Eshdat L, Berger H, Hopf H, Rabinovitz M (2002) J Am Chem Soc 124:3822
14. Alabugin IV, Kovalenko SV (2002) J Am Chem Soc 124:9052
15. Alabugin IV, Manoharan M (2003) J Am Chem Soc 125:4495
16. Nash JJ, Squires RR (1996) J Am Chem Soc 118:11872
17. Davidson ER, Borden WT (1983) J Phys Chem 87:4783
18. Cohen RD, Sherrill CD (2001) J Chem Phys 114:8257
19. Crawford TD, Stanton JF, Allen WD, Schaefer III HF (1997) J Chem Phys 107:10626
20. Stanton JF (2001) J Chem Phys 115:10382
21. Russ NJ, Crawford TD, Tschumper GS (2005) J Chem Phys 120:7298
22. Löwdin P-O (1963) Rev Mod Phys 35:496
23. Eisfeld W, Morokuma K (2000) J Chem Phys 113:5587
24. Crawford TD, Kraka E, Stanton JF, Cremer D (2001) J Chem Phys 114:10638

25. Wladyslawski M, Nooijen M (2002) In ACS Symposium Series, Vol. 828, pp 65–92,
26. Slipchenko LV, Krylov AI (2006) J Phys Chem A 110:291
27. Krishnan R, Binkley JS, Seeger R, Pople JA (1980) J Chem Phys 72:650
28. Frisch MJ, Pople JA, Binkley JS (1984) J Chem Phys 80:3265
29. Woon DEJr, Dunning TH (1994) J Chem Phys 80:3265
30. Cristian AMC, Shao Y, Krylov AI (2004) J Phys Chem A 108:6581
31. Purvis GD, Bartlett RJ (1982) J Chem Phys 76:1910
32. Raghavachari K, Trucks GW, Pople JA, Head-Gordon M (1989) Chem Phys Lett 157:479
33. Sherrill CD, Krylov AI, Byrd EFC, Head-Gordon M (1998) J Chem Phys 109:4171
34. Nooijen M, Bartlett RJ (1995) J Chem Phys 102:3629
35. Krylov AI (2001) Chem Phys Lett 338:375
36. Levchenko SV, Krylov AI (2004) J Chem Phys 120:175
37. Becke AD (1993) J Chem Phys 98:5648
38. Arnold DW (1994)PhD Thesis, UC Berkeley
39. Shao Y, Head-Gordon M, Krylov AI (2003) J Chem Phys 118:4807
40. NBO 50 Glendening ED, Badenhoop JK, Reed AE, Carpenter JE, Bohmann JA, Morales CM, Weinhold F (2001) Theoretical Chemistry Institute, University of Wisconsin, Madison, WI
41. Mulliken RS (1955) J Chem Phys 23:1997
42. Kong J, White CA, Krylov AI, Sherrill CD, Adamson RD, Furlani TR, Lee MS, Lee AM, Gwaltney SR, Adams TR, Ochsenfeld C, Gilbert ATB, Kedziora GS, Rassolov VA, Maurice DR, Nair N, Shao Y, Besley NA, Maslen P, Dombroski JP, Daschel H, Zhang W, Korambath PP, Baker J, Bird EFC, Van Voorhis T, Oumi M, Hirata S, Hsu C-P, Ishikawa N, Florian J, Warshel A, Johnson BG, Gill PMW, Head-Gordon M, Pople JA (2000) J Comput Chem 21:1532
43. ACES II Stanton JF, Gauss J, Watts JD, Lauderdale WJ, Bartlett RJ (1993) The package also contains modified versions of the MOLECULE Gaussian integral program of J Almlöf and PR Taylor, the ABACUS integral derivative program written by TU Helgaker, HJAa Jensen, P Jørgensen and PR Taylor, and the PROPS property evaluation integral code of PR Taylor
44. Helgaker T, Jørgensen P, Olsen J (2000) Molecular electronic structure theory. Wiley, New York
45. Munsch TE, Slipchenko LV, Krylov AI, Wenthold PG (2004) J Org Chem 69:5735
46. Bally T, Sastry GN (1997) J Phys Chem A 101:7923
47. Polo V, Kraka E, Cremer D (2002) Molecular Physics 100:1771
48. Zhang Y, Yang W (1998) J Chem Phys 109:2604
49. Lundber M, Siegbahn PEM (2005) J Chem Phys 122:1
50. Reed DR, Hare M, Kass SR (2000) J Am Chem Soc 122:10689
51. Slipchenko LV, Krylov AI (2002) J Chem Phys 117:4694